correspondence

The dynamics of Van Allen belts revisited

To the editor — In an effort to explain the formation of a narrow third radiation belt at ultra-relativistic energies detected during a solar storm in September 2012¹, Mann et al.² present simulations from which they conclude it arises from a process of outward radial diffusion alone, without the need for additional loss processes from higher frequency waves. The comparison of observations with the model in Figs 2 and 3 of their Article clearly shows that even with strong radial diffusion rates, the model predicts a third belt near $L^* = 3$ that is twice as wide as observed and approximately an order of magnitude more intense. We therefore disagree with their interpretation that "the agreement between the absolute fluxes from the model and those observed by REPT [the Relativistic Electron Proton Telescope] shown on Figs 2 and 3 is excellent."

Previous studies³ have shown that outward radial diffusion plays a very important role in the dynamics of the outer belt and is capable of explaining rapid reductions in the electron flux. It has also been shown that it can produce remnant belts (Fig. 2 of a long-term simulation study⁴). However, radial diffusion alone cannot explain the formation of the narrow third belt at multi-MeV during September 2012. An additional loss mechanism is required.

Higher radial diffusion rates cannot improve the comparison of model presented by Mann *et al.* with observations. A further increase in the radial diffusion rates (reported in Fig. 4 of the Supplementary Information of ref. 2) results in the overestimation of the outer belt fluxes by up to three orders of magnitude at energy of 3.4 MeV.

Observations at 2 MeV, where belts show only a two-zone structure, were not presented by Mann et al. Moreover, simulations of electrons with energies below 2 MeV with the same diffusion rates and boundary conditions used by the authors would probably produce very strong depletions down to L = 3-3.5, where L is radial distance from the centre of the Earth to the given field line in the equatorial plane. Observations do not show a non-adiabatic loss below $L \sim 4.5$ for 2 MeV. Such different dynamics between 2 MeV and above 4 MeV at around L = 3.5 are another indication that particles are scattered by electromagnetic ion cyclotron (EMIC) waves that affect only energies above a certain threshold.

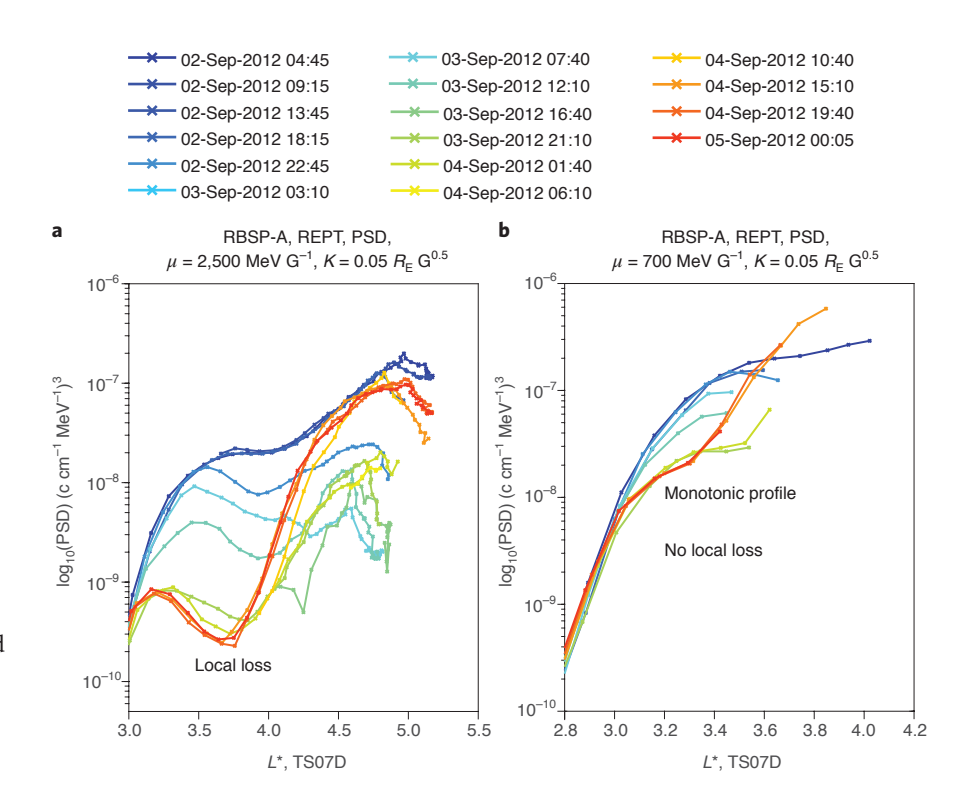


Figure 1 | Time evolution of radiation profiles in electron PSD at relativistic and ultra-relativistic energies. **a**, Similar to Supplementary Fig. 3 of ref. 2, but using TSO7D model¹⁰ and for μ = 2,500 MeV G⁻¹, K = 0.05 $R_{\rm E}$ (where $R_{\rm E}$ is the radius of the Earth). **b**, Similar to Supplementary Fig. 3 of ref. 2, but using TSO7D model and for μ = 700 MeV G⁻¹, corresponding to MeV energies in the heart of the belt. Minimum in PSD in the heart of the multi-MeV electron radiation belt between 3.5 and 4 $R_{\rm E}$ deepening between the afternoon of 3 September and 5 September clearly show that the narrow remnant belt at multi-MeV below 3.5 $R_{\rm F}$ is produced by the local loss.

Observations of the phase space density (PSD) provide additional evidence for the local loss of electrons. Around $L^* = 3.5-4$ PSD shows significant decrease by an order of magnitude starting in the afternoon of 3 September (Fig. 1a), while PSD above $L^* = 4$ is increasing. The minimum in PSD between $L^* = 3.5-4$ continues to decrease until 4 September. This evolution demonstrates that the loss is not produced by outward diffusion. Radial diffusion cannot produce deepening minima, as it works to smooth gradients. Just as growing peaks in PSD show the presence of localized acceleration⁵, deepening minima show the presence of localized loss.

The minimum in the outer boundary is reached on the evening of 2 September. After that, the outer boundary moves up, while the minimum decreases by

approximately an order of magnitude, clearly showing that this main decrease cannot be explained by outward diffusion, and requires additional loss processes. The analysis of profiles of PSD is a standard tool used, for example, in the study about electron acceleration⁵ and routinely used by the entire Van Allen Probes team. In the Supplementary Information, we show that this analysis is validated by using different magnetic field models. The Supplementary Information also shows that measurements are above background noise.

Deepening minima at multi-MeV during the times when the boundary flux increases are clearly seen in Fig. 1a. They show that there must be localized loss, as radial diffusion cannot produce a minimum that becomes lower with time. At lower energies of 1–2 MeV, which corresponds to

lower values of the first adiabatic invariant μ (Fig. 1b), the profiles are monotonic between $L^* = 3-3.5$, consistent with the absence of scattering by EMIC waves that affect only electrons above a certain energy threshold⁶⁻⁹.

In summary, the results of the modelling and observations presented by Mann *et al.* do not lend support to the claim of explaining the dynamics of the ultrarelativistic third Van Allen radiation belt in terms of an outward radial diffusion process alone. While the outward radial diffusion driven by the loss to the magnetopause² is certainly operating during this storm, there is compelling observational and modelling^{2,6} evidence that shows that very

efficient localized electron loss operates during this storm at multi-MeV energies, consistent with localized loss produced by EMIC waves.

References

- 1. Baker, D. N. et al. Science 40, 186-190 (2013).
- 2. Mann, I. R. et al. Nat. Phys. 12, 978-983 (2016).
- 3. Shprits, Y. Y. et al. J. Geophys. Res. 111, A11214 (2006).
- Subbotin, D. A., Shprits, Y. Y. & Ni, B. J. Geophys. Res. 116, A12210 (2011).
- 5. Reeves, G. D. et al. Science 341, 991–994 (2013)
- Shprits, Y. Y. et al. Nat. Phys. 9, 699–703 (2013).
 Shprits, Y. Y. et al. Nat. Commun. 7, 12883 (2016).
- 8. Shprits, Y. Y., Kellerman, A., Aseev, N., Drozdov, A. Y. &
- Shprits, Y. Y., Kellerman, A., Aseev, N., Drozdov, A. Y. & Michaelis, I. Geophys. Res. Lett. 44, 1204–1209 (2017).
- 9. Ma, Q. et al. Geophys. Res. Lett. 42, 987-995 (2015).
- Tsyganenko, N. A. & Sitnov, M. I. J. Geophys. Res. 112, A06225 (2007).

Additional information Supplementary information is available on the online version of the paper.

Yuri Y. Shprits^{1,2,3*}, Richard B. Horne⁴, Adam C. Kellerman³ and Alexander Y. Drozdov³ ¹Helmholtz Centre Potsdam, GFZ, German Research Centre For Geosciences, 14473 Potsdam, Germany. ²University of Potsdam, 14469 Potsdam, Germany. ³Department of Earth, Planetary, and Space Sciences, University of California, Los Angeles, California 90095, USA. ⁴British Antarctic Survey, Cambridge CB3 0ET, UK. *e-mail: yshprits@gfz-potsdam.de

Mann et al. reply — We are pleased to address the comment on our paper¹ from Shprits *et al.*² since we believe it supports our conclusion that magnetopause shadowing and ultralow-frequency (ULF) wave outward transport can drive fast losses into the heart of the ultra-relativistic electron radiation belt and produce a remnant belt. As reported by Baker et al.3, the September 2012 geomagnetic storm produced this phenomena, and we showed¹ how such losses could explain it. However, Shprits et al. claim that for this single specific storm that electromagnetic ion cyclotron (EMIC) wave losses are essential for explaining the observed third belt. We dispute this interpretation.

Contrary to the claims of Shprits et al., outward ULF wave radial diffusion can act on sufficiently short timescales4 to generate the observed remnant belt. For example, Supplementary Fig. 1 displays additional magnetopause shadowing simulation runs using the same approach described in ref. 1 showing an erosion of the outer belt and the generation of both monotonic and non-monotonic PSD profiles without invoking EMIC wave effects. Our ULF wave-driven radiation belt simulations not only reproduce the third belt morphology but also produce a narrower remnant belt at higher energies just as observed (Supplementary Fig. 2).

The principal argument for the action of EMIC wave loss in the Shprits *et al.* Correspondence is based on analysis of electron phase space density (PSD) profiles. However, we disagree with their analysis and the derived PSD profiles since they do not appear to take into account uncertainties in measurements at the lowest REPT instrument energy channels,

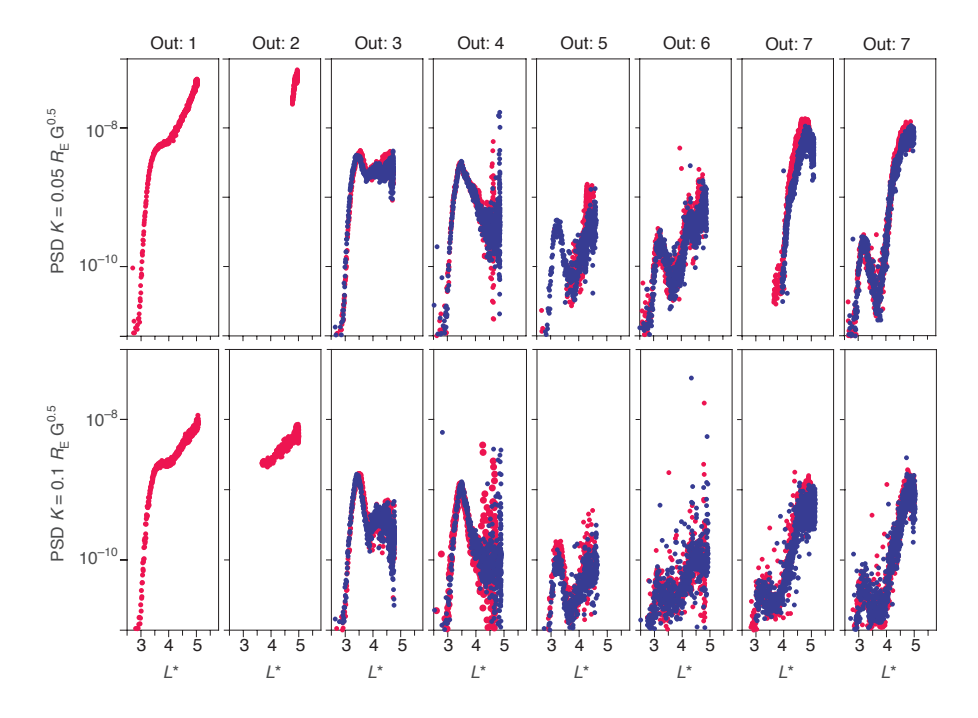


Figure 1 | Equatorial PSD profiles at fixed $K = 0.05 R_E G^{0.5}$ and $0.1 R_E G^{0.5}$ at fixed $\mu = 3,500$ MeV G^{-1} from outbound passes of Van Allen Probes A (red) and B (blue). The interval shown spans 00 UT on 2 September 2012, to 12 UT on 4 September 2012. The losses associated with decreasing PSD profiles with L^* around outbound orbits 3 and 4 are consistent with magnetopause shadowing and fast outward ULF wave radial transport. Similar behaviour is seen for the inbound passes, and also during inbound and outbound passes at 2,500 MeV G^{-1} . See Supplementary Figs 3–6 and related Supplementary Information for more details.

and effects from off-equatorial orbits (discussed in more detail in Supplementary Information). Figure 1 shows outbound Van Allen probe PSD profiles as a function of L^* at fixed first adiabatic invariant $\mu=3,500~{\rm MeV~G^{-1}}$, and at two fixed second invariant $K=0.05~R_{\rm E}~{\rm G}^{0.5}$ and 0.1 $R_{\rm E}~{\rm G}^{0.5}$. This indicates a different sequence of events to those advanced by Shprits et al. Instead,

it shows the development of PSD profiles that decrease with L^* consistent with loss from magnetopause shadowing and ULF wave enhanced outward radial diffusion, a ~2.5 orders of magnitude decrease in PSD seen at L^* ~ 5 from the initial conditions to the time of outbound orbit 4 at both K. See also Supplementary Figs 3 and 4, and 5 and 6, which show further data in support

correspondence

of this conclusion from both inbound and outbound orbits at 3,500 MeV G^{-1} and 2,500 MeV G^{-1} , respectively. A smaller local dip in PSD is seen later in the evolution, and as discussed in the Supplementary Information might be related to EMIC wave losses, but this weaker loss is not responsible for creating the third belt morphology.

Observations from multiple additional spacecraft such as the Los Alamos geosynchronous spacecraft (reaching L^* as low as ~4.5; Supplementary Fig. 7 and the constellation of GPS satellites (Supplementary Figs 8 and 9) are also consistent with losses from enhanced outward ULF transport and magnetopause shadowing.

Overall, our analysis indicates that our original conclusion in ref. 1 remains valid — the remnant belt and third belt morphology can be created by fast outward ULF wave transport and magnetopause shadowing, without resorting to a requirement for EMIC wave losses.

References

- 1. Mann, I. R. et al. Nat. Phys. 12, 978-983 (2016).
- Shprits, Y. Y., Horne, R. B., Kellerman, A. C. & Drozdov, A. Y. Nat. Phys. 14, XXX–XXX (2017).
- 3. Baker, D. N. et al. Science 340, 186-190 (2013).
- Mann, I. R. & Ozeke, L. G. J. Geophys. Res. Space Phys. 121, 5553–5558 (2016).

Acknowledgements

I.R.M. is supported by a Discovery Grant from Canadian NSERC. S.K.M. is supported by US Department of Energy Laboratory Directed Research and Development

(LDRD) award 20150127ER. I.J.R. is funded by STFC grant ST/L000563/1 and NERC grant NE/L007495/1. KRM is supported by an NSERC Postdoctoral Fellowship. CARISMA is operated by the University of Alberta, funded by the Canadian Space Agency. We acknowledge the WDC for Geomagnetism, Kyoto University, Japan, for the geomagnetic indices. This work was supported by RBSP-ECT funding provided by JHU/APL Contract No. 967399 under NASA's Prime Contract No. NAS5-01072. The Sub-Auroral Magnetometer Network (SAMNET) is operated by the Space Plasma Environment and Radio Science (SPEARS) group, Department of Physics, Lancaster University, UK. We thank the institutes who maintain the IMAGE Magnetometer Array. We thank the CXD team at LANL, the SOPA PI (Michael Henderson) and ESP PI (Gregory Cunningham) for providing the energetic electron data.

Data availability statement

Magnetometer data is available from the Canadian Array for Realtime Investigations of Magnetic Activity (http://www.carisma.ca). Other magnetometer data is available from SAMNET and IMAGE, and from the SuperMAG consortium (http://supermag.jhuapl.edu). The GPS CXD data used in the work are archived by NOAA's NCEI and indexed at data.gov (as detailed in Morley et al. 2017). LANL SOPA and ESP data can be made available upon request from LANL (requests to Mike Henderson (mghenderson@lanl.gov), and Greg Cunningham (cunning@lanl.gov), respectively). Relativistic Electron Proton Telescope (REPT) data is available from the Energetic Particle, Composition, and Thermal Plasma (ECT) suite on Radiation Belt Storm Probes (RBSP) (http://www.rbsp-ect.lanl.gov). Solar wind, GOES satellite data is available from the National Centers for Environmental Information (http://satdat.ngdc.noaa. gov/sem/goes/data/new_full/), THEMIS data from the Space Physics Data Facility of the Goddard Space Flight Center (http://cdaweb.gsfc.nasa.gov/), and geomagnetic indices from the World Data Center for Geomagnetism, Kyoto (http://wdc.kugi.kyoto-u.ac.jp/). All other data supporting the findings of this study are available from the authors upon request.

Additional Information

Supplementary information is available on the online version of the paper.

I. R. Mann¹, L. G. Ozeke¹, S. K. Morley², K. R. Murphy^{1,3}, S. G. Claudepierre⁴, D. L. Turner⁴, D. N. Baker⁵, I. J. Rae⁶, A. Kale¹, D. K. Milling¹, A. J. Boyd^{7,8}, H. E. Spence⁷, H. J. Singer⁹, S. Dimitrakoudis^{1,10}, I. A. Daglis^{11,10} and F. Honary¹²

¹Department of Physics, University of Alberta, Edmonton, Alberta T6G 2G7. Canada. ²Space Science and Applications (ISR 1), Los Alamos National Laboratory, Los Alamos, New Mexico 87545, USA. 3NASA Goddard Spaceflight Center, Code 674, Greenbelt, Maryland 20771, USA. 4The Aerospace Corporation, Los Angeles, California 90009, USA. 5Laboratory for Atmospheric and Space Physics, University of Colorado, Boulder, Colorado 80309, USA. 6Mullard Space Science Laboratory, University College London, Holmbury St Mary, Dorking, Surrey RH5 6NT, UK. 7Institute for the Study of Earth, Oceans, and Space, University of New Hampshire, Durham, New Hampshire 03824-3525, USA. 8The New Mexico Consortium, Los Alamos, New Mexico 87544, USA. 9Space Weather Prediction Center, NOAA, Boulder, Colorado, 80305, USA. 10 National Observatory of Athens, Institute for Astronomy, Astrophysics, Space Applications and Remote Sensing, 15236 Penteli, Greece. ¹¹Department of Physics, National and Kapodistrian University of Athens, 15784 Athens, Greece. 12 Department of Physics, Lancaster University, Lancaster LA1 4YB, UK.

e-mail: imann@ualberta.ca